Designing Nanostructured Strontium Aluminates particles for Achieve High Luminescence Properties

R.E. Rojas-Hernandez[*], M.A. Rodriguez , F. Rubio-Marcos, A. Serrano, J. F. Fernandez

Electroceramic Department, Instituto de Cerámica y Vidrio, CSIC, Kelsen 5, 28049, Madrid, Spain.

Abstract

The synthesis of submicron phosphorescent particles has been widely studied in the last decade due to the promising industrial applications of these materials. Several matrices have been developed; being the $SrAl_2O_4$ doped with Eu^{2+} and Dy^{3+} the most strongly researched owing to its better stability and longer afterglow than other matrices. However, the powders produced by different synthesis routes have a particle size within the range of 20 to 100 μm. In view of practical use, the reduction of the particle size of such material is not clear up to date. To reach the objective to synthesize submicron particles, in the present study the powders have been synthesized by a combustion method and has carried out a dry grinding process. Optimizing the synthesis, that is, understanding the effect of the fuel (urea) on the phase formation, it has been possible to control the reaction and to achieve high luminescence properties. Besides, a dry grinding process has carried out to decrease the particle size and to avoid the moisture presence during grinding. A correlation between the presence of secondary phases and the Eu^{2+} content have been evaluated and therefore the phosphors are treated in N_2-H_2 atmosphere to obtain an enhancement of the crystallinity simultaneous to the increase of the photoluminescence. The significance of this work lies in evaluating whether such a material can be practically used or not. We believe such a material might be the most promising candidate for replacing phosphors micron-particles in some areas in the future.

---

[*] Corresponding author. Tlf: +34 91 735 58 40; Ext 1074. Fax: +34 91 735 58 43. E-mail address:rociorojas@icv.csic.es (R.E. Rojas-Hernandez)

1. Introduction.

Strontium aluminate family hosts are attractive because exhibit excellent phosphorescence properties and have good stability [1–4]. These functional inorganic materials have a wide field of application in persistent luminous paints, inks, ceramics [5–7]. After the discovery in 1996 of $SrAl_2O_4$: $Eu^{2+}Dy^{3+}$ as new persistent luminescent compound by Matsuzawa et al. [8], many researchers have developed some methods for preparation of these powders including sol-gel method, hydrothermal synthesis, chemical precipitation, laser synthesis and solid-state reaction. However, the powders have large particle size that is unpractical for printing applications in which particles <10 µm are required. Solid state reaction particles, for example, requires high temperatures , typically 1300- 1900°C, long processing time and as result the average size is ranged 20-100 µm [9–11] .

Combustion technique appears to be a promising route for the preparation of different powders. This route is versatile, rapid and requires low temperatures (600°C), allows uniform doping in a single step and it is not necessary a reductive atmosphere to prepare the powders [12–14]. The particles obtained by usual combustion method are in the range of nanometers, the particles are largely agglomerated, nonetheless less dense and highly sintered in relation to particles obtained by others methods [14,15].

Luminescent properties depend considerably on the grain size; attractive applications will be possible if the grain size decreases. For that, after selecting the processing parameters to obtain the phosphors, a dry grinding process is proposed to avoid the contact of the powder with liquid media and to minimize the moisture content. It is known that strontium aluminates have a weak water resistance, as a consequence a liquid media containing water is a drawback for this class of phosphors [16]. The low energy dry grinding is used to disperse nanoparticles in microparticles [17,18].

Herein, we present a facile method to design $SrAl_2O_4$:Eu^{2+}, Dy^{3+} nanostructured powders with well-regulated $SrAl_2O_4$/Eu^{2+}, Dy^{3+} ratios, which are synthesized by a combustion method. The main achievements are related to the morphology-inheriting mechanism to obtain $SrAl_2O_4$:Eu^{2+}, Dy^{3+} nanostructured powders with target particle size in the submicron range, and to develop of a key synthesis route for accurate composition control $SrAl_2O_4$/Eu^{2+}, Dy^{3+} ratios. It should be emphasized that the $SrAl_2O_4$:Eu^{2+}, Dy^{3+} nanostructured powders with the adequate particle size exhibit a significant high photoluminescence based on the elimination of Eu^{3+} -rich secondary phases.

2. Experimental details.

Synthesis: $SrAl_2O_4{:}Eu^{2+}$, Dy^{3+} particles were synthesized via solution combustion synthesis. The solution was prepared by dissolving Al $(NO_3)_3{\cdot}9H_20$ (Merck, 98.5%) in deionized water and $SrCO_3$ (Merck, 99.9%), Eu_2O_3 (Metal Rare Earth Limited, 99.5%), Dy_2O_3 (Rare Earth Limited, 99.5%) in nitric acid HNO_3 to form nitrate solution. The above materials were mixed according to the chemical formula $Sr_{1-x-y}Eu_xDy_yAl_2O_4$, where x = 0.02 and y= 0.01. The solution was stirred during 30 min under heating at 80 ºC, after that, urea was added in a ratio of 3 times of the stoichiometric quantity. The full precursor solution was dried at 100ºC in a porcelain crucible with a glass-watch lid. The solution was introduced into a furnace maintained at 400ºC and heated up to 600°C; where the ignition took place in a few minutes (ca. 10 min). A white powder with an extremely porous and foam structure was obtained.

The powder synthesized by combustion method was milled to reduce the particle size. A dry grinding method was carried out. The dry grinding process consisted of shaking the powder obtained by combustion synthesis adding ZrO_2 balls with a diameter of 0.5 mm in a 60 cm^3 nylon container for 5 min, 10 min, 15 min, 20 min and 25 min at 50rpm using a turbula-type mixer. Grinded powders were thermally treated at 900ºC in a furnace under N_2-H_2 atmosphere in order to improve the luminescent properties.

Structural and Microstructural Characterization: The phase identification of the powders was determined by X-ray diffraction (XRD, D8, Bruker) using Cu Kα. Crystallite size (D) of the powders was estimated from the full width at half maximum of the diffraction peak using the Sherrer's equation (after correction of the data by the instrumental broadening of the system):

$$D = \frac{K\lambda}{B\cos\theta}$$

(1)

where λ is the X-ray wavelength, B half maximum of the diffraction peak, θ is the angle of diffraction, and using a shape factor (K) of 0.9. Pseudo-Voigt peak function were used for deconvolution of XRD peak profiles in the region between 27-31º 2θ, this function is a combination of Lorentzian and Gaussian functions that describes diffraction profiles from crystalline materials. Profile de-convolution was carried out using the Origin Lab V8.5 software to resolve the presence of different contribution; the overall goodness of the fit after convergence is specified by the adjusted R-square factor. Particle size distribution measurements of the phosphor powders were determined by laser diffraction (Mastersizer S, Malvern, U.K.). Measurements of d_{50}

(median particle size), d_{90} (the particle size where 90% of the particles are below that size) and d_{10} (the particle size where 10% of the particles are below that size) were made. Surface area measurements were performed using a 3-point BET technique (Quantachrome Instruments, Florida, USA). The morphology of the nanostructured powders was evaluated using secondary electron images of field emission scanning electron microscopy (FE-SEM, Hitachi S-4700). The particle size and morphology at the nanoscale of the samples were also evaluated using a transmission electron microscope (TEM/HRTEM, JEOL 2100F) operating at 200 kV and equipped with a field emission electron gun providing a point resolution of 0.19 nm. The microscope is coupled with an INCA x-sight energy dispersive X-ray spectrometer (EDXS, Oxford Instruments) used for chemical elemental analysis. Additional chemical analyses were performed by inductively coupled plasma-optical emission spectroscopy (ICP-OES, PerkinElmer Optima 3300DV).

Optical Characterization: Optical properties of these materials were investigated by measuring emission and excitation spectra. The photoluminescence spectra of the phosphor particles were recorded with a spectrofluorometer (Fluorolog®-3, HORIBA Jobin Yvon) at room temperature. The luminescence intensity was measured over the wavelength 425–650 nm, a Xenon arc lamp was used as an excitation source (λ_{exc}= 380nm and 464nm). In order to correlate, X-ray absorption measurements were carried out at the Spanish CRG beamline BM25 (SpLine ESRF). X-ray absorption spectroscopy (XAS) spectra at Eu L3-edge were performed at room temperature and in fluorescence mode. The fluorescence signal was collected using a 13 element Si (Li) solid state detector from 2 eV Scientific Instruments. An average of three XAS scans was carried out for all samples. The X-ray absorption data were analysed with a standard procedure using ATHENA software [19].

3. Results

3.1. Structural, microstructural, and optical characterization of the SrAl$_2$O$_4$: Eu^{2+}, Dy^{3+} phosphors synthesized by combustion method.

Combustion synthesis consist of a reaction in homogenous solution of oxidizers and a fuel. There are various available fuels that can be used such as glycine. Citric acid or urea to initiate decomposition reaction. However, it has been reported that using glycine as fuel has a number of difficulties in the combustion process and the cost of the synthesis increases because the cost of glycine is much higher than urea [20]. For these reasons, urea was selected as combustion fuel. It should be noted that introducing of urea means introduce energy in the system and for that has an important role in the reaction [21]. Previous studies established that

maximum amount of urea, as 2.5 times the stoichiometric amount in order to achieve the formation of monoclinic phase [22]. The urea is a reducing agent, when it is incorporated in the reaction needs an oxidant agent to complete the reaction; the oxygen of the medium fulfills this role. Probably if the ratio of urea increases greatly the oxygen of the medium is not enough to complete the reaction. In order to attain a complete reaction during the combustion process the addition of nitric acid is here proposed as an internal oxidizing agent accordingly with the following reaction:

$$5CO(NH_2)_2 + 6HNO_3 \rightarrow 5CO_2 + 13H_2O + 8N_2 \tag{1}$$

The amount of urea included in the system required a stoichiometric amount of nitric acid accordingly to the above equation. Firstly, to synthesize the phosphors it has been introduced three times of the theoretical quantity of urea and addition of the corresponding HNO_3 amount. The introduction of a slight excess of urea as fuel has an important effect on the phase formation, but larger urea amounts inhibited the strontium incorporation into the tridymite-like structure. In this way, in this work the presence of an oxidizing agent promotes both an effective completion of the reaction and a higher crystalline order in strontium aluminate phase ($SrAl_2O_4$:Eu^{2+}, Dy^3). The main intention using HNO_3 in excess was to fulfill the reaction. This approach provides a mechanism to manage the reaction conditions. It is important to remark that it is necessary to modify the process to achieve the self sustained combustion. Different techniques have been used to try to manage the reaction; for example using ammonium nitrate and glycine as a fuel [23]. These new strategies favor the synthesis process efficiently and open new insights to tune the reaction.

A basic identification of the structure and of the symmetry of the powders obtained by combustion synthesis is made according to X-Ray Diffraction, XRD. The X-ray diffraction pattern of the combustion powders is shown in Fig. 1, the XRD pattern shows characteristic peaks of the $SrAl_2O_4$ monoclinic phase (space group $P2_1$), whose pattern is characterized by three peaks centered in the 2θ range $28°$ to $30°$ and matched with the $SrAl_2O_4$ standard values give in JCPDS (No. 34-0379). Besides, XRD pattern also unveils details of the slight appearance of $SrCO_3$ phases. As a consequence, the most probable origin of this behaviour must be related to the carbonation of the nitrate species owing to the reaction medium created by carbon dioxide during the combustion. In addition, some minority secondary phases are present as $Sr_3Al_2O_6$ and $Sr_4Al_{14}O_{25}$. The presence of these secondary phases is attributed to the characteristic lack of energy homogeneity during the combustion reaction [21]. The $Sr_3Al_2O_6$ phase appears at lower temperatures in the $SrO-Al_2O_3$ system than $SrAl_2O_4$ phase [24]. Also, the $Sr_4Al_{14}O_{25}$ phase can be associated to the reduced

temperature range of stability for the monoclinic polymorph which implies the presence of $Sr_4Al_{14}O_{25}$ phase [25]. The synthesis must take in account two aspects the fuel ratio and the initiating temperature. The latter aspect has been evaluated to select the optimal temperature. Fig. 1 exhibits the XRD patterns of the $SrAl_2O_4$ powders synthesized by combustion process when incorporates nitric acid as an oxidizing agent with the urea content of m=3, and initiation combustion temperatures of 400, 500 and 600ºC. The results obtained show that the powder does not achieve a good ignition at 400ºC; impurity phase, $Sr_3Al_2O_6$, appears. Only after increasing the temperature, the impurity phase decreases at 500ºC and almost disappears at 600ºC. Therefore, the temperature of 600ºC has been chosen to induce the self-combustion synthesis.

The crystallite size is ca. 36 nm of the powders by using the Sherrer's equation on crystallographic planes (-221), (220), (211) and (031) for the monoclinic phase. This value indicates the formation of crystal structure with a limited coherent range typically of nanoparticles.
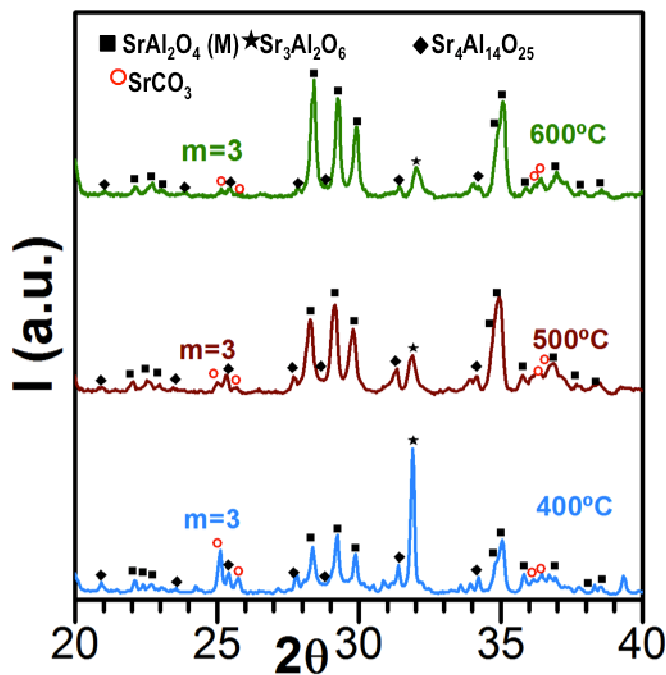

Figure 1. XRD pattern of $SrAl_2O_4$:Eu, Dy phosphor synthesized by the combustion process with a quantity of urea , m=3 and by adding HNO_3 at 400, 500 and 600ºC.

The above structural characterization confirms the successful formation of the $SrAl_2O_4$ phase with a monoclinic symmetry after the combustion process. Fig. 2(a-g) shows sequential images of the morphology of the synthesized powders and their luminescent properties. Fig. 2(a) shows a photograph of the as resulted

powders after the ignition process. So, a white powder with an extremely porous and foam structure is obtained.
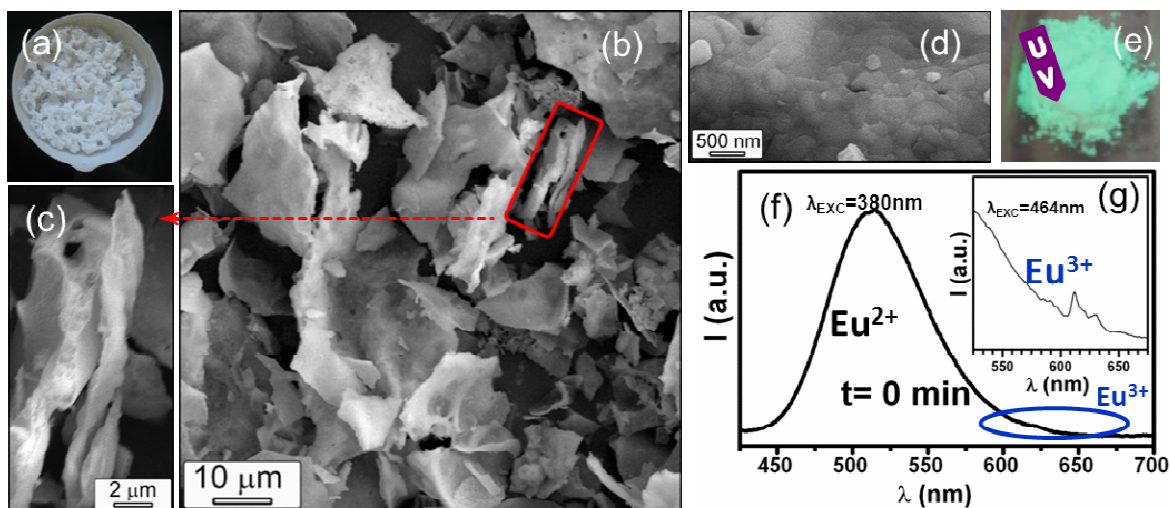

Figure 2. (a) Photograph of $Sr_{0,97}Al_2O_4$:$Eu_{0,02}$, $Dy_{0,01}$ powder obtained after the synthesis; **(b, c)**FE-SEM micrographs of flakes powders obtained by combustion synthesis with sizes of 5-25 μm; **(d)** Detail of nanostructured sheet; **(e)** Green phosphorescent emission after UV illumination of the powder; **(f)** Emission spectra of the $Sr_{0,97}Al_2O_4$:$Eu_{0,02}$, $Dy_{0,01}$ including upon excitation at 380 nm and **(g)** 464 nm.

The FE-SEM micrographs, shown in Fig. 2 (b-d), illustrate the morphology and particle size distribution of the $SrAl_2O_4$: Eu, Dy sample. From Fig. 2(b), it can be observed that the $SrAl_2O_4$: Eu, Dy sample has a typical morphology produced by combustion method, which consisting mainly in flakes shaped with sizes of 5-25 μm. The spongy material formed has voids and pores attributed to the escape of large volume of gasses during the reaction. A more exhaustive inspection of the morphology of the flakes reveals that they are nanostructured; see Figs. 2(c) and (d). Besides, these nanostructured sheets have a ≤ 1 μm in thickness which it is an interesting dimensional size for many applications.

The main optical response of the $Sr_{0,97}Al_2O_4$:$Eu_{0,02}$, $Dy_{0,01}$ powder is presented in the Figs. 2(e, f, g). Fig. 2(f) shows the photoluminescence emission spectra of $Sr_{0,97}Al_2O_4$:$Eu_{0,02}$, $Dy_{0,01}$ powder. The emission band centered at 510 nm are assigned to the spin-allowed transition of $4f^65d^1 \rightarrow 4f^7$ ($^8S_{7/2}$) of Eu^{2+} ions, whereas the emission located at 611nm correspond to the spin-forbidden transition of $^5D_0 \rightarrow ^7F_2$ for the Eu^{3+} ions [26], see Fig. 2(g). The photoluminescence emission effects on the powders are also reflected macroscopically. So, the Fig. 2(e) shows a photograph of the resultant powders emitting in the green phosphorescent region after UV illumination of the powder.

3.2. Influence of the Particle Size in the Functional Properties of the SrAl$_2$O$_4$: Eu^{2+}, Dy^{3+} phosphors.

As it has been explained in the introduction section, the luminescent properties depend considerably on the particle size; attractive applications will be possible if the particle size decreases. To verify that the luminescent properties are strongly influenced by the particle size of the Sr$_{0,97}$Al$_2$O$_4$:Eu$_{0,02}$, Dy $_{0,01}$ phase, additional experiments are performed with the aim to reduce the particle size. The combustion powder as obtained by the combustion process is crushed in an Agatha mortar and is milled by the dry grinding process. In order to characterize the effect of the grinding time on the particle size, the powders are collected at different grinding times from 5 min to 25 min, and the particle size distribution is analyzed. Results are shown in Fig. 3(a,b), after t$_1$=5 min of grinding, the average particle size of the product becomes ~8 µm; being a great decrease in the value in a few minutes. The reduction of the average particle size is clearly more effective during the initial phase of the process, t$_3$=15 min. After t$_4$=20 min the particle size decreases more steadily and the behavior of the particle size reduction becomes to follow an asymptotic tendency. The behavior of the particle size distribution can be clearly observed in Fig. 3(b) . It is noticeable first that the milling process allows a gradual decrease in particle size and secondly the great decrease in the value of d$_{90}$, from 62 to 10 µm. The ungrinded powder has a starting BET surface area of 0.45 m^2/g, while surface areas of the milling powder increase until 1.11, 2.27, 2.90, 3.28 and 3.50 m^2/g for milling times grinded at 5, 10, 15, 20 and 25, respectively. This increment can be explained due to the decrease of particle size.
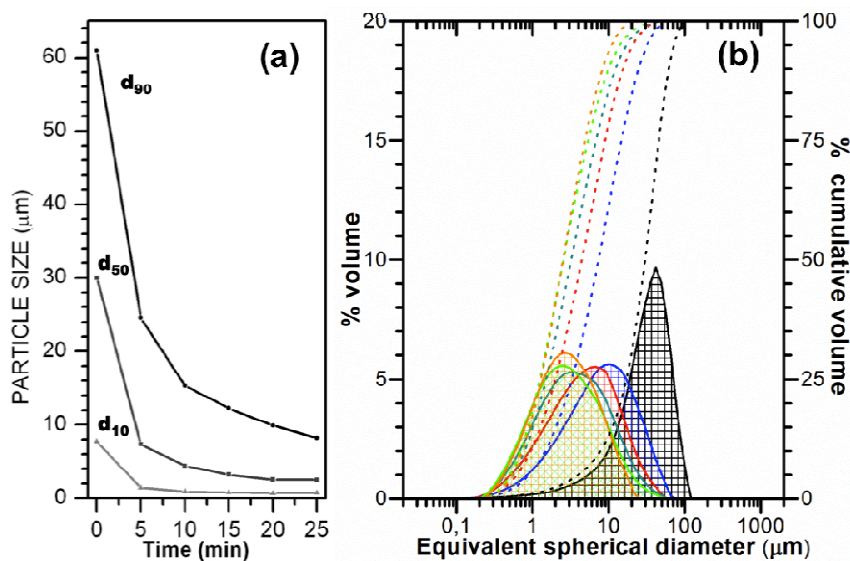

Figure 3. (a) Evolution of the particle size as a function of the grinding time and **(b)** particle-size distribution of milled powders at 5, 10, 15, 20 and 25 minutes.
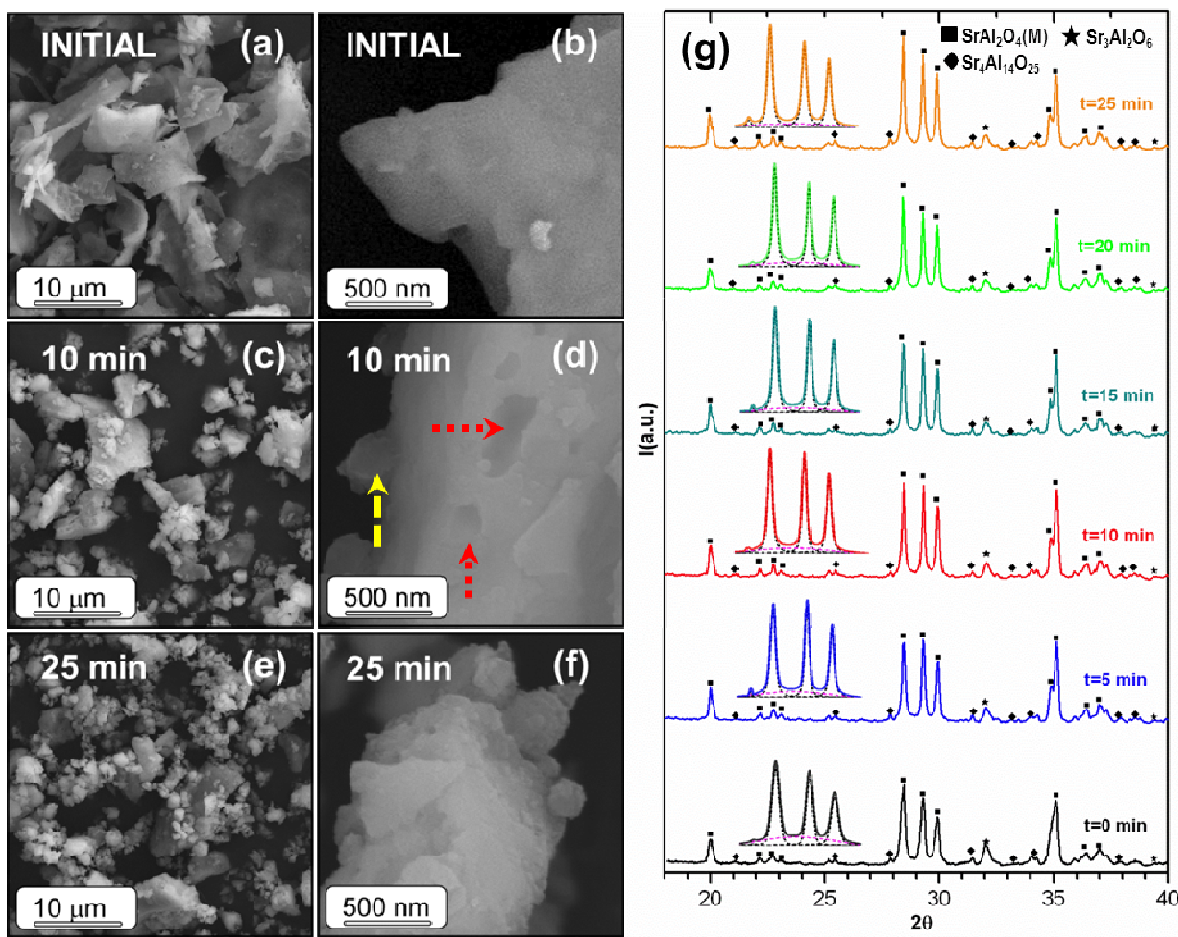
Figure 4. FE-SEM micrographs of powders obtained by combustion synthesis **(a,b)** after dry grinding process during 10 min **(c,d)** and 25 min **(e,f)** ; **(g)** Initial XRD pattern corresponding to the combustion powders after dry grinding process during 5, 10, 15, 20 and 25 minutes. The inset in (g) shows the deconvolution of XRD peak profiles in the region between 27-31° 2θ.

To investigate the effect of the grinding time on the morphology of the $SrAl_2O_4$: Eu^{2+}, Dy^{3+} phosphors, the powders are subsequently observed by FE-SEM. Fig. 4(a-f) includes the FE-SEM images of the initial combustion powder and the particles after the grinding process for 10 and 25 min. The size reduction that occurred for grinding procedures is also revealed from this experimental measurement. The flake-like shape of $SrAl_2O_4$: Eu^{2+}, Dy^{3+} phosphors prepared via combustion route is greatly reduced to 5µm after 10 min. Besides, during the grinding a delamination of the flakes is produced too. After 25 min the grinding produces a particle size decrease, obtaining particles with an average size $\leq 0.5µm$, which are slightly agglomerated. From the perspective of the morphology, two remarkable observations can be made. Firstly, the $SrAl_2O_4$: Eu^{2+}, Dy^{3+} phosphors evolved towards a lower average particle size by the grinding time provoking a delamination of the original flakes-like particle; and secondly, large grinding time generates the formation of defects in the flakes-like particle surface, as shown in the Figures 4(d) and (f). These defects are caused by

9

energy impacts produced during the milling process, causing the generation of highly reactive surfaces, as signaled with yellow and red arrows, respectively.

Although morphological information on the $SrAl_2O_4$: Eu^{2+}, Dy^{3+} phosphors obtained by FE-SEM is invaluable, the FE-SEM technique yields no or very limited structural information. So, the grinding time effect on the structure of the $SrAl_2O_4$: Eu^{2+}, Dy^{3+} phosphors is also evaluated by XRD technique. The X-ray powder diffraction patterns of $SrAl_2O_4$: Eu^{2+}, Dy^{3+} grinded at 5, 10, 15, 20 and 25 min are shown in Fig. 4 (g). The patterns of all the grinded powders show the diffraction peaks corresponding to $SrAl_2O_4$ phase, which possess monoclinic symmetry. This fact is important due to the grinding process do not affect to the optically active phase, which is associated to the monoclinic symmetry in this system.

From the luminescence spectra in Fig. 5(a), it can see that the luminescence intensity of $SrAl_2O_4$: Eu^{2+}, Dy^{3+} grinded decreases as the grinding time increases. The photoluminescence intensity (PL) and the particle size, $d_{50,}$ as a function of the grinding time are plotted in Fig. 5 (b). The degradation of the photoluminescence of the powders can be attributed to a structural damage during the grinding. While the observed average particle size appeared to have been successfully reduced by the grinding, the surface of the particles is altered; probably a surface amorphization occurred due to the impacts produced during grinding process and the oxidation of Eu^{2+} increases because there is a higher active surface that can be hydrolyzed in the presence of moisture.

Another important feature of the XRD of the nanostructure is that X-ray diffraction powder reflections over the range between 27.5–30.5° 2θ have a broad background, revealing the existence of two contributions; the presence of particles nanostructured and particles with incomplete crystallization or a mixing material with a certain degree of amorphicity. A closer look of the diffraction patterns shows a change in the width of the peaks patterns and a decrease of the background located below these reflections during the grinding process. The grinding stage modifies the sample crystallinity (D). To demonstrate this behavior, we have estimated the D from the peaks ranging between 27.5-30.5° and 34°-36° 2θ values, which are well resolved. Grinding process will tend to reduce the crystallite size; however Fig. 5(c) shows that the crystallite size grows in the first stage c.a. 54 nm (t1=5min) and after that the value remains constant. A possible explanation for unusually crystallite growth might be related to the relaxation of the lattice, the particles are initially highly strained due to the inherent synthesis process and the grinding process allows relaxing the lattice strain, therefore the crystallite size increase. Moreover, it does not appear a great reduction of the crystallite size

after 10 min, which suggest that the grinding process has low energy to break up the crystallites. To evaluate these two contributions, previously mentioned, also it has been carried out a deconvolution of XRD peak profiles in the 2 region 27-31°. The results are shown in the inset in Fig. 4(g); obtaining values of adjusted R-square of 0.9872, 0.995, 0.9934, 09936, 0.9922, 0,9923 to the powders after dry grinding process during 5, 10, 15, 20 and 25 minutes, respectively; the results demonstrate the goodness of the fit. The pseudo–Voigt function corresponding to the total XRD pattern ($\square$) as well as the deconvoluted individual peaks (---) are shown in the inset in figure 4(g). It has been evaluated the ratio (% Crystalline phase) between the sum of the area under the four peaks at 27.85, 28.42, 29.28 and 29.92 2θ and the area under the peak at 28.96 (broad peak); this ratio represents the crystallinity of the powder. As can be seen in Fig. 5(c), this ratio increases highly in the first stage and increases gradually after 10 min , which can be related to the transformation from the strained to relaxed state in the crystal lattice. These results are in good agreement with crystallite size and particle size measurements, showing that the initial stage implies the reduction of particles size not breaking the crystallite and relaxation of the crystal. Therefore the crystallinity percent is higher after 5 min compared with the particles before the grinding process.

Finally, the patterns do not reveal a noticeable amorphization of the powder during the dry grinding process, which could be expected considering that it is a low energy process.
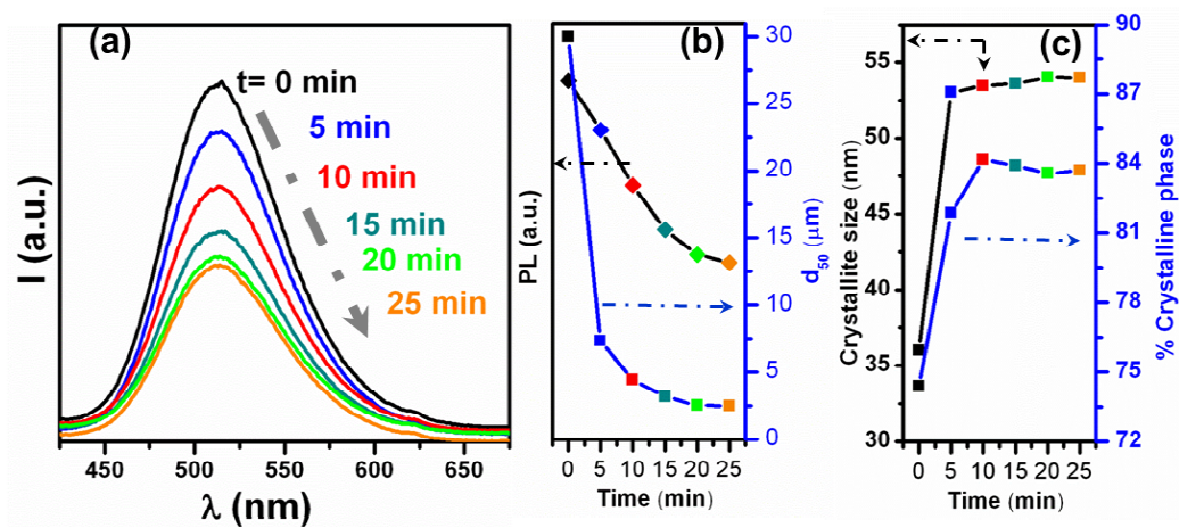

Figure 5. (a) Comparison of PL emission spectra of the $Sr_{0,97}Al_2O_4:Eu_{0,02}$, $Dy_{0,01}$ as synthesized and after dry grinding process during 5, 10, 15, 20 and 25 minutes, upon excitation at 380 nm; **(b)** PL and particle size, d_{50} (median particle size) as a function of time of grinding process; **(c)** Crystallite size and percent of crystalline phase as a function of time of grinding process.

3.3. Exploring Different Annealing Atmospheres to Improve the Photoluminescence of the SrAl$_2$O$_4$: Eu^{2+}, Dy^{3+} phosphors.

It should be noted that the particles size of the powder is greatly reduced after 15 min, therefore in order to improve the emission intensity a thermal treatment is proposed. The powder grinding for 15 min is treated at 900°C in N$_2$-H$_2$ atmosphere. As a result, it can be observed in the emission spectra Fig. 6(a) that the intensity of the emission increases, which might be associated with the reduction of defects created on the surface by the grinding process and to the enhancement of the crystalline quality.

It is interesting to note that the subsequent thermal treatment originates an emission in the red region Fig. 6(b). The emission spectrum excited by visible light (λ_{exc} = 464 nm) includes a broad-band peaked at 605 nm ascribes to the $^5D_0$-$^7F_2$ transition. It could be attributed to the presence of the SrAl$_4$O$_7$: Eu^{2+} as secondary phase [27,28]. Nevertheless the presence of this phase is really low and the dominant phase is the monoclinic SrAl$_2$O$_4$. Of course, the detailed reasons need to be further investigated, and the relative research is under processing.
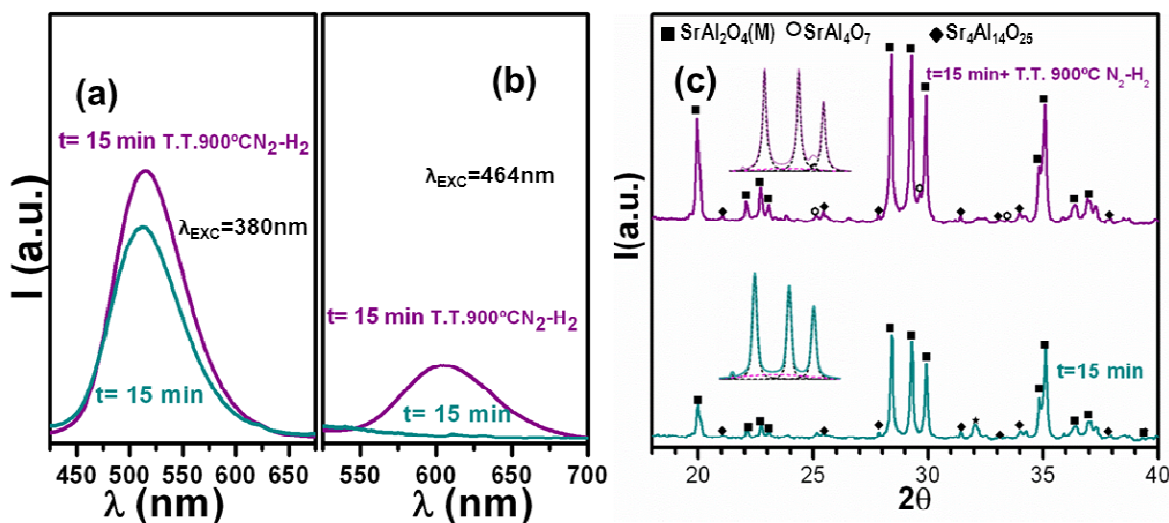

Figure 6. Emission spectra of the Sr$_{0,97}$Al$_2$O$_4$:Eu$_{0,02}$, Dy$_{0,01}$ powders after dry grinding process during 15 minutes (t$_3$) and the same powder after a thermal treatment at 900°C in N$_2$-H$_2$ atmosphere (t$_3$ + T.T. 900°C N$_2$-H$_2$), upon excitation at 380 nm **(a)** and 464 nm **(b)**. XRD pattern corresponding to the combustion powders after dry grinding process during 15 and the same powder after a thermal treatment at 900°C in N$_2$-H$_2$ atmosphere **(c)**.The inset in **(c)** shows the deconvolution of XRD peak profiles in the region between 27-31° 2θ.

In order to clarify the annealing atmosphere effect on the structure of the SrAl$_2$O$_4$: Eu^{2+}, Dy^{3+} phase, and their morphological structure, we have carried out a TEM characterization on the SrAl$_2$O$_4$: Eu^{2+}, Dy^{3+} sample series. So, TEM studies are also carried out to characterize the morphology and grain size of synthesized

powder after grinding and after a thermal treatment. Fig. 7 shows the TEM images of the powder obtained by combustion synthesis after grinding during 15 min. From Fig. 7a, the high agglomeration and heterogeneous distribution of the nanostructured phosphor can be clearly observed. These nanostructured particles have a broad average particle size in the range between 50 and 90 nm, Fig. 7(a); consisting mainly in nanosize grains of 55 nm , which is in good agreement with that estimated by Scherer formula. Moreover, energy dispersive spectra (EDS) experiments are carried out to determine the chemical composition of the particles. EDS analysis in the point 1 taken from the powder matches to the theoretical composition of $SrAl_2O_4$: Eu^{2+}, Dy^{3+} phase, Fig. 7 (a). By selecting an area on the edge of the particle it can observe an amorphous region as a result of the grinding process, Fig. 7 (b). EDS measurement at the point 2 differs from the theoretical composition; the composition is rich in Al.
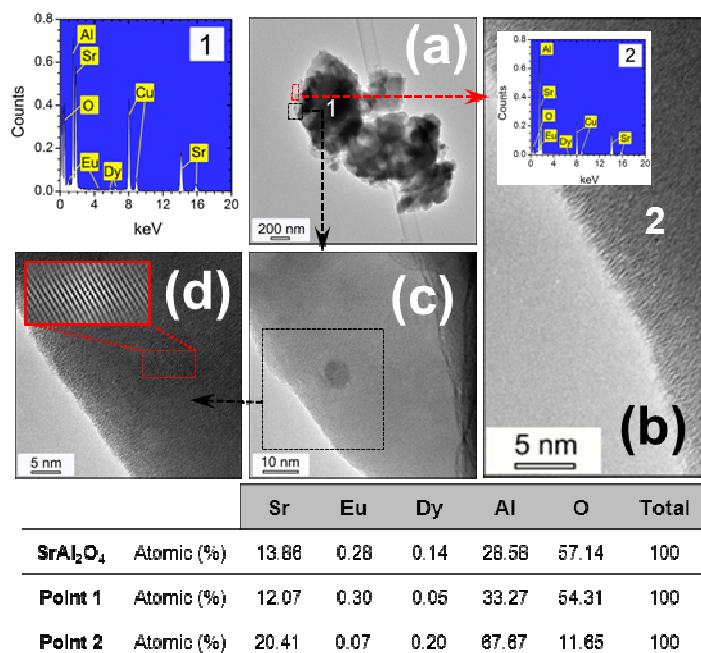

		Sr	Eu	Dy	Al	O	Total
$SrAl_2O_4$	Atomic (%)	13.86	0.28	0.14	28.58	57.14	100
Point 1	Atomic (%)	12.07	0.30	0.05	33.27	54.31	100
Point 2	Atomic (%)	20.41	0.07	0.20	67.67	11.65	100

Figure 7. TEM images and EDS analysis of $Sr_{0,97}Al_2O_4$:$Eu_{0,02}$, $Dy_{0,01,}$ after a dry grinding process during 15 min. **(a)**Agglomerated particles;**(b)** EDS analysis in the outer area of the particle (Point 2); **(c)** Detail of agglomerated particles **(d)** Detail of nanoparticle and the inset is the lattice fringe image of the area of interest, the d-spacing is 4.045 Å. The inset of the Fig. **(d)** shows the inverse FFT of the selected area in panel c to identify the crystallographic planes and interplanar distance in a $Sr_{0,97}Al_2O_4$:$Eu_{0,02}$, $Dy_{0,01}$ nanoparticle. Table shows the composition on the points shown in the panels **(a)** and **(b)** derived from EDS spectra, which represent the atomic percentages of each element.

The micrograph with higher magnifications, Fig. 7(c) shown the presence of major phase ($SrAl_2O_4$: Eu^{2+}, Dy^{3+}) covered by the minor amorphous phase, in which can be identified the presence of nanoparticles with an average size of about 5-10 nm, see Fig. 7(c). The HR-TEM image (Fig. 7.d) and the inverse FFT pattern

(insert of the Fig. 7.d) show the lattice planes, and the interplanar spacing is calculated to be 4.045 Å, that correspond to the (-111) reflection of the $SrAl_2O_4$ pattern JCPDS (No. 34-0379) .
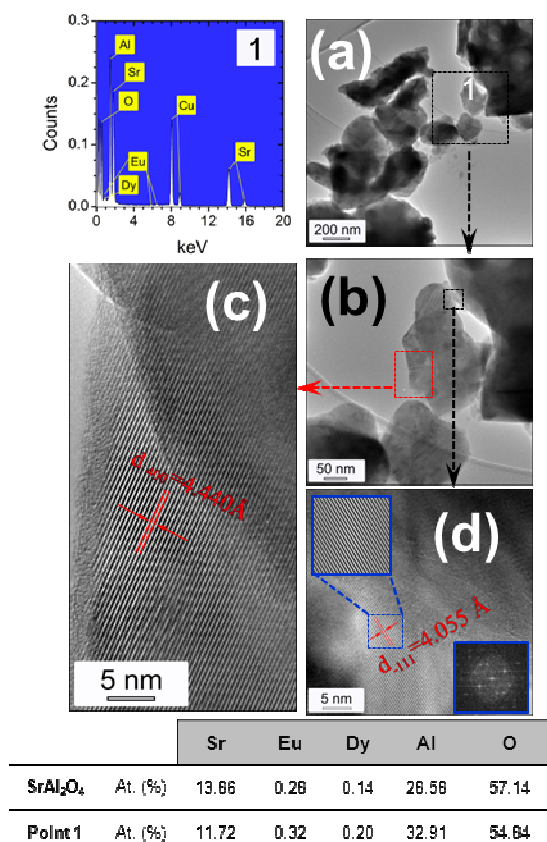

		Sr	Eu	Dy	Al	O
$SrAl_2O_4$	At. (%)	13.86	0.28	0.14	28.58	57.14
Point 1	At. (%)	11.72	0.32	0.20	32.91	54.84

Figure 8. TEM images and EDS analysis of $Sr_{0.97}Al_2O_4:Eu_{0.02}$, $Dy_{0.01}$ after a dry grinding process during 15 min and thermally treated at 900°C in N_2-H_2 atmosphere. **(a)**Agglomerated particles;**(b)** Detail of agglomerated particles; **(c)** The lattice fringe image, the d-spacing is 4.440 Å corresponding to $SrAl_4O_7$.;**(d)** The lattice fringe image of the area of interest, the d-spacing is 4.055 Å. The inset is the Fast Fourier Transform (FFT) of the image. Table shows the composition in the point shown on the panels **(a)** derived from EDS spectrum, which represents the atomic percentages of each element.

To evaluate the effect of annealing conditions (in N_2-H_2 atmosphere) on the morphology and composition of the $SrAl_2O_4$: Eu^{2+}, Dy^{3+} is also studied by TEM. TEM images of phosphors treated at 900°C are shown in Fig. 8. Figures 8(a) and (b) shows low-magnification images where the $SrAl_2O_4$: Eu^{2+}, Dy^{3+} structure can be clearly observed. The EDS analysis in the point 1 confirms that the average atomic composition is consistent with the theoretical composition of $SrAl_2O_4$: Eu^{2+}, Dy^{3+}. We note from the HRTEM image in Fig.8(c) that the crystallinity of particles largely increase. Thus, the detailed observation of the phosphors treated reveals a good crystalline structure. As a relevant result, we found that the amorphous phase, which covered the grinded particles (Fig. 7c) disappears with the thermal treatment at 900°C in a N_2-H_2 atmosphere. This fact suggests that the annealing process favors the re-crystallization of the amorphous phase.

Another experimental proof of the higher crystallinity of phosphors is found from the HRTEM images of the Fig. 8 (c) where it can be observed crystalline planes of the $SrAl_2O_4$: Eu^{2+}, Dy^{3+} monoclinic phase. Thus, the interplanar distance measured from TEM image in Fig. 8 (c) and Fig. 8 (d) is 4.440 and 4.055 Å, respectively, and these distances are associated with (440) plane in $SrAl_4O_7$ and (-111) plane in $SrAl_2O_4$. The presence of this secondary phase $SrAl_4O_7$ is correlated with the results obtained by XRD (Fig. 6(c)). The high crystallinity demonstrates the assignment to the emission at 605 nm attributed to this secondary phase. It can be observed, from the inset of Fig. 8 (d), the corresponding FFT pattern that indicates $SrAl_2O_4$ phosphor with good crystallinity. The crystallite size increase being c.a. 58 nm and the percent of crystalline phase is higher after the thermal treatment, obtaining a value of 93, 01% and adjusted R-square of 0.9874.
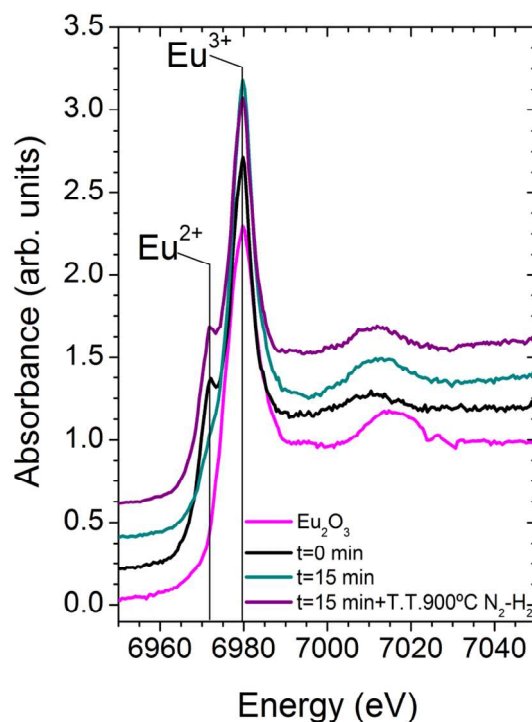

Figure 9. XANES spectra of $Sr_{0,97}Al_2O_4$:$Eu_{0,02}$, $Dy_{0,01}$ powders prepared before (t=0), after dry grinding process for 15 min (t=15 min) and after dry grinding process for 15 min and a post- thermal treatment at 900°C in N_2-H_2 atmosphere. The Eu_2O_3 reference is shown as well.

The broad band centered at 510 nm in the photoluminescence emission spectra of $Sr_{0,97}Al_2O_4$:$Eu_{0,02}$, $Dy_{0,01}$ powders synthesized, as shown in Fig. 6, indicates the reduction of Eu^{3+} to Eu^{2+} and the substitution of Sr^{2+} sites by Eu^{2+}. In order to check out the oxidation state of Europium in the system, and to obtain information about its local environment, a XANES study is performed. This reduction can also be confirmed by X-Ray Absorption Near Edge Spectroscopy (XANES) at Eu-L_3 edge. The measured XANES spectra at Eu-L_3 edge of

the samples synthesized and the Eu_2O_3 reference (reference foil) are shown in Fig. 9. It is well-known that the peaks located at 6972 and 6979.7 eV are assigned to the divalent and trivalent oxidation state of europium ions, respectively [29]. The energy difference between both edges is around 7.7 eV. The comparison of the white line transitions between both edges allows estimating the relative fraction between Eu^{2+} and Eu^{3+} in each sample. The XANES spectrum of the initial powder (t=0) clearly indicates that the divalent and trivalent europium coexist in the powder. After grinding the powder during 15 min (t=15min) the Eu^{3+} edge increases and the Eu^{2+} edge decreases, indicating that Eu^{2+} ions are oxidized during the milling. The origin of such behavior is attributed to the alteration of the particle surface provoking the amorphization of the $SrAl_2O_4$: Eu^{2+}, Dy^{3+} particles, which may produce the partial oxidation of the Eu^{2+} to Eu^{3+} ions on the $SrAl_2O_4$: Eu^{2+}, Dy^{3+} surface particles. Whereas, the thermal treatment at 900°C in a N_2-H_2 atmosphere implies that Eu^{3+} ions can be reduced. The powder grinded during 15 min and thermal treated exhibit a reduction of Eu^{3+} ions to Eu^{2+} due to the annealing process in N_2-H_2. And therefore, the annealing process in reducing atmospheres improves the optical response on the $SrAl_2O_4$: Eu^{2+}, Dy^{3+} system, because it produces the selective reduction of the Eu^{3+} to Eu^{2+} ions in addition of the increasing in crystallinity.

4. Conclusions

$SrAl_2O_4$:Eu^{2+}, Dy^{3+} is successfully synthesized by combustion method by incorporation of higher quantities of urea and addition HNO_3 as oxidant agent to complete the reaction and promote the formation of monoclinic $SrAl_2O_4$ phase. Nanostructured sheets prepared via combustion route with a thickness ≤ 1μm are obtained by a dry grinding process to reduce the particle size. Despite the degradation of the photoluminescence by the grinding process, the resulted powders have good optical properties. A correlation with the appearance of secondary amorphous phase with presence of Eu^{3+} is observed. High phosphorescence properties of submicron powders are obtained after post-thermal treatment in reducing atmosphere due to the increase of crystallinity and the reduction of Eu^{3+} to Eu^{2+}. The submicron size of the nanostructured particles allows their use in applications which required low particles size and high phosphorescence properties. Overall, $SrAl_2O_4$: Eu^{2+}, Dy^{3+} nanostructured particles shows good photoluminescence response and maybe the optimum phosphor candidate for replacing conventional micrometric-sized phosphors in some practical applications.

5. Acknowledgments

References

[1] F.C. Palilla, A.K. Levine, M.R. Tomkus, Fluorescent Properties of Alkaline Earth Aluminates of the Type MAl_2O_4 Activated by Divalent Europium, J. Electrochem. Soc. 115 (1968) 642–644.

[2] V. Abbruscato, Optical and Electrical Properties of $SrAl_2O_4$:Eu^{2+}, J. Electrochem. Soc. 118 (1971) 930–933.

[3] T. Aitasalo, P. Dereń, J. Hölsä, H. Jungner, J.-C. Krupa, M. Lastusaari, et al., Persistent luminescence phenomena in materials doped with rare earth ions, J. Solid State Chem. 171 (2003) 114–122.

[4] J. Hölsa, H. Jungner, M. Lastusaari, J. Niittykoski, Persistent luminescence of Eu^{2+} doped alkaline earth aluminates, J. Alloy. Compd. 324 (2001) 326–330.

[5] H. Yina, J. Xinye, C. Qiang, L. Ding, W. Farong, PMMA with Long-Persistent Phosphors and Its Behavior of Luminescence, J. Rare Earths. 24 (2006) 157–159.

[6] B. Karasu, S.Y. Kaya, Process parameters determination of phosphorescent pigment added, frit-based wall tiles vetrosa decorations, Ceram. Int. 38 (2012) 2757–2766.

[7] D.M. Van Duynhoven, Tintable luminescent paint US Patent No. 6359048, (2002).

[8] T. Matsuzawa, Y. Aoki, N. Takeuchi, Y. Murayama, A New Long Phosphorescent Phosphor with High Brightness, $SrAl_2O_4$:Eu^{2+},Dy^{3+}, J. Electrochem. Soc. 143 (1996) 2670.

[9] X. Luo, W. Cao, Z. Xiao, Investigation on the distribution of rare earth ions in strontium aluminate phosphors, J. Alloys Compd. 416 (2006) 250–255.

[10] E. Scimce, Phase studies of $SrO-Al_2O_3$ by emission signatures of Eu^{2+} and Eu^{3+}, Mater. Res. Bull. 32 (1997) 337–341.

[11] J. Sanchez-Benitez, A. de Andrés, M. Marchal, E. Cordoncillo, M.V. Regi, P. Escribano, Optical study of $SrAl_{1.7}B_{0.3}O_4$:Eu, R (R=Nd, Dy) pigments with long-lasting phosphorescence for industrial uses, J. Solid State Chem. 171 (2003) 273–277.

[12] S.T. Aruna, A.S. Mukasyan, Combustion synthesis and nanomaterials, Curr. Opin. Solid State Mater. Sci. 12 (2008) 44–50.

[13] Z. Qiu, Y. Zhou, M. Lu, A. Zhang, Q. Ma, Combustion synthesis of three-dimensional reticular-structured luminescence $SrAl_2O_4$: Eu , Dy nanocrystals, Solid State Sci. 10 (2008) 629–633.

[14] Y. Lin, Z. Zhang, F. Zhang, Z. Tang, Q. Chen, Preparation of the ultrafine $SrAl_2O_4$: Eu , Dy needle-like phosphor and its optical properties, Mater. Chem. Phys. 65 (2000) 103–106.

[15] Z. Qiu, Y. Zhou, M. Lü, A. Zhang, Q. Ma, Combustion synthesis of three-dimensional reticular-structured luminescence $SrAl_2O_4$:Eu,Dy nanocrystals, Solid State Sci. 10 (2008) 629–633.

[16] Y. Zhu, M. Zheng, J. Zeng, Y. Xiao, Y. Liu, Luminescence enhancing encapsulation for strontium aluminate phosphors with phosphate, Mater. Chem. Phys. 113 (2009) 721–726.

[17] I. Lorite, a. Campo, J.J. Romero, J.F. Fernández, Isolated NAnoparticle Raman Spectroscopy, J. Raman Spectrosc. 43 (2012) 889–894.

[18] F. Rubio-marcos, C. V Manzano, J. Reinosa, J.J. Romero, P. Marchet, M.S. Mart, et al., Mechanism of Ni 1 À x Zn x O Formation by Thermal Treatments on NiO Nanoparticles Dispersed over ZnO, (2011) 13577–13583.

[19] B. Ravel, M. Newville, ATHENA, ARTEMIS, HEPHAESTUS: Data analysis for X-ray absorption spectroscopy using IFEFFIT, in: J. Synchrotron Radiat., 2005: pp. 537–541.

[20] S.M. Maliyekkal, Anshup, K.R. Antony, T. Pradeep, High yield combustion synthesis of nanomagnesia and its application for fluoride removal., Sci. Total Environ. 408 (2010) 2273–82.

[21] M. a. Rodríguez, C.L. Aguilar, M. a. Aghayan, Solution combustion synthesis and sintering behavior of $CaAl_2O_4$, Ceram. Int. 38 (2012) 395–399.

[22] E. Shafia, M. Bodaghi, M. Tahriri, The influence of some processing conditions on host crystal structure and phosphorescence properties of $SrAl_2O_4$: Eu^{2+}, Dy^{3+} nanoparticle pigments synthesized by combustion technique, Curr. Appl. Phys. 10 (2010) 596–600.

[23] K. V Manukyan, Y. Chen, S. Rouvimov, P. Li, X. Li, S. Dong, et al., Ultrasmall α-Fe$_2$O$_3$ Superparamagnetic Nanoparticles with High Magnetization Prepared by Template-Assisted Combustion Process, (2014).

[24] P. Escribano, M. Marchal, M. Luisa Sanjuán, P. Alonso-Gutiérrez, B. Julián, E. Cordoncillo, Low-temperature synthesis of SrAl$_2$O$_4$ by a modified sol–gel route: XRD and Raman characterization, J. Solid State Chem. 178 (2005) 1978–1987.

[25] E. Cordoncillo, B. Julian-Lopez, M. Martínez, M.L. Sanjuán, P. Escribano, New insights in the structure–luminescence relationship of Eu:SrAl$_2$O$_4$, J. Alloys Compd. 484 (2009) 693–697.

[26] H. Zeng, Z. Lin, Q. Zhang, D. Chen, X. Liang, Y. Xu, et al., Green emission from Eu^{2+}/Dy^{3+} codoped SrO-Al$_2$O$_3$-B$_2$O$_3$ glass-ceramic by ultraviolet light and femtosecond laser irradiation, Mater. Res. Bull. 46 (2011) 319–322.

[27] S. Yesilay Kaya, E. Karacaoglu, B. Karasu, Effect of Al/Sr ratio on the luminescence properties of SrAl$_2$O$_4$:Eu^{2+}, Dy^{3+} phosphors, Ceram. Int. 38 (2012) 3701–3706.

[28] W.M. Yen, M.J. Weber, Inorganic Phosphors: Compositions, Preparation and Optical Properties, The CRC Pr, 2004.

[29] N. Avci, K. Korthout, M. a. Newton, P.F. Smet, D. Poelman, Valence states of europium in CaAl$_2$O$_4$:Eu phosphors, Opt. Mater. Express. 2 (2012) 321.
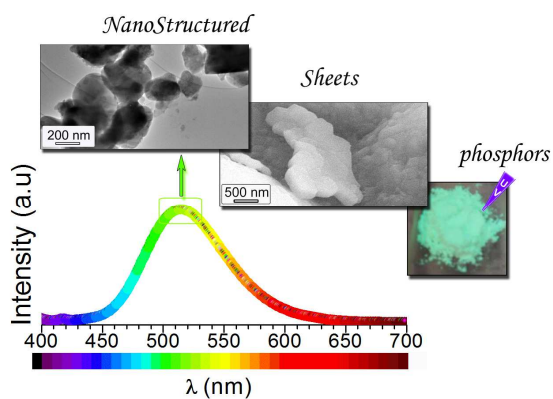
The table of contents (TOC)

By

R.E. Rojas-Hernandez[*], M.A. Rodriguez , F. Rubio-Marcos, A. Serrano, J. F.

Fernandez

ToC figure

[*] Corresponding author. Tlf: +34 91 735 58 40; Ext 1074. Fax: +34 91 735 58 43. E-mail address:rociorojas@icv.csic.es (R.E. Rojas-Hernandez)